International Forum on Aeroelasticity and Structural Dynamics
IFASD 2024
17-21 June 2024, The Hague, The Netherlands

RAYLEIGH-RITZ METHOD WITH MULTIBODY DYNAMICS FOR HIGHLY FLEXIBLE STRUCTURES

Leonardo Barros da Luz[1], **Flávio Luiz Cardoso-Ribeiro**[1], **Pedro Paglione**[1]

[1]Instituto Tecnológico de Aeronáutica
São José dos Campos, São Paulo, 12228-900.
leobdl.formula@gmail.com
flaviocr@ita.br
pedro.paglione@gmail.com

Keywords: Multibody, Rayleigh-Ritz method, High Flexible, Structural dynamics

Abstract: Flexible structures are increasingly prevalent in the commercial aviation industry, and the use of highly flexible structures is a prominent trend for the future. When analyzing those structures, it is crucial to consider geometric nonlinearities caused by large displacements. This means that the modeling of the structures must incorporate nonlinear structural models, which can lead to a reasonable increase in computational costs. To tackle this challenge, a framework has been developed for static and dynamic analyses of highly flexible structures. It is based on a linear structural model, utilizing the Rayleigh-Ritz method, coupled with multibody dynamics. The geometric nonlinearities are modeled through rigid connections between multiple flexible bodies that form the final structure. Two different approaches have been used for the multibody dynamics. The former considers all degrees of freedom of each body and solves only the kinematics of the constraint to maintain the connections between the bodies, which resulted in an augmented system with Lagrange multipliers that can be used to reconstruct forces and moments of constraint. The latter utilizes only the independent degrees of freedom whilst reconstructing the dependent ones through the equations that define the constraints between the bodies, directly solving the constraints. The results obtained show that proposed framework accurately describes the dynamics of highly flexible structures and can be used to simulate structures with various types of connections, showcasing its versatility for other applications like simulations of morphing structures such as wings with folding wingtips.

NOMENCLATURE

$\overline{R}$	=	Indicates that the variable is a matrix
$\mathbf{R}$	=	Indicates that the variable is a vector
$\mathbf{R}^i$	=	Indicates that the vector $\mathbf{R}$ is written in the frame i
$\mathbf{R}_{O,j}$	=	Indicates that the vector $\mathbf{R}$ is the vector with respect to the origin O of the body j
$\widetilde{\mathbf{R}}$	=	Skew-symmetric matrix of vector $\mathbf{R}$, which represents a cross product

1 INTRODUCTION

Flexible structures are becoming increasingly common in the commercial aviation industry, and the utilization of highly flexible structures is a prominent trend for the future. Additionally, in other applications such as unmanned aircraft missions at high altitudes with a high level of

autonomy, it is crucial to employ wings with exceptionally high elongation, as demonstrated in NASA's Helios project. When examining these structures, it is important to consider geometric nonlinearities [1].

In the work of Ref. [1], comparisons were made between geometrically nonlinear and linear models using X-HALE, aircraft presented in [2], with three wing lengths, 4 meters, 6 meters and 8 meters. The authors concluded that it is necessary to use geometrically non-linear models as the wing length increases.

To analyze structures with geometric nonlinearities, Refs. [3–5] have developed nonlinear structural models. These models alone can accurately describe the deflection of the structure, taking into account large displacements. In the study conducted by Esteban, a combination of a multibody model and a linear finite element model was utilized to depict geometrically nonlinear effects. Similarly, in the works of [6, 7], the multibody model was coupled with rigid beam segments using revolution joints and equivalent springs to simulate flexible behavior. Furthermore, [7] also presented an alternative model wherein a modal analysis of a finite element structure is performed, and the resulting model is incorporated into the multibody simulation.

In this work, unlike the previously cited literature, we employ a flexible multibody modeling approach coupled with the Rayleigh-Ritz method, evaluating different function bases for analyzing highly flexible structures.

This paper is structured into three main sections, each focusing on a distinct aspect of the proposed framework. Section 2 delves into flexible multibody modeling, detailing the connections between bodies. Section 2.2 presents the structural modeling, outlining the derivation of stiffness and damping matrices and the relationship between flexible and rigid body degrees of freedom. These sections lay the foundational elements for understanding the framework. Finally, Section 3 discusses the verification and results.

2 MODELING

In this section, the modeling framework is presented. Firstly, in Subsection 2.1 the multibody approach is detailed. Then, 2.2 details the structural model used to represent each flexible body, including the shape functions and the stiffness matrix.

2.1 Dynamic Model

The dynamics modeling approach selected for this study is based on multibody theory, described in [8]. This choice was made based on its ability to precisely simulate the dynamic behavior of interconnected bodies subjected to various types of constraints.

2.1.1 Reference frames

The motion of a body is represented by the translation and rotation of the body frame in relation to the inertial frame. The body frame j, illustrated in Fig. 1, is fixed on the body j with its origin not necessarily coincident with the center of mass. The inertial frame, denoted by i, is fixed to an initial position.

To describe vectors from the inertial frame to the body frame of the body j, the rotation matrix $\overline{A}_{j/i}$ is used considering the conventional rotation sequence 3-2-1 [8], the same is valid for the body k.

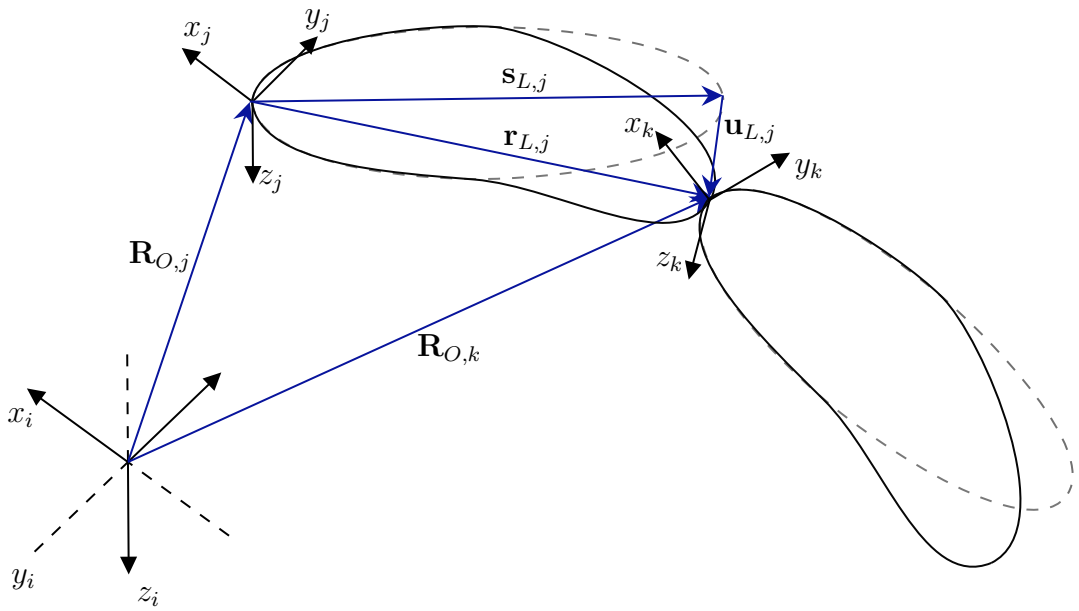

Figure 1: **Definition of the inertial frame and the body frame, with their representative vectors.**

2.1.2 Influence of deformation degrees of freedom

A body, because it is a continuous medium, has infinite degrees of freedom, which in practice is unfeasible to analyze computationally. So, to make the analysis feasible, shape functions are used which allow the interpolation of the displacement field with a finite number of degrees of freedom [8].

The matrix of shape functions $\overline{N}(\mathbf{s}_p)$ varies only spatially and when applied to the point P defined by the vector $\mathbf{s}_p$ of the undeformed body gives the elastic displacement $\mathbf{u}_p$, as

$$\mathbf{u}_p(\mathbf{s}_p, t) = \overline{N}(\mathbf{s}_p)\mathbf{q}_j(t) \tag{1}$$

where $\mathbf{q}_j$ are time-varying amplitudes that represent flexible degrees of freedom for the body j.

Thus, the total displacement of point P is

$$\mathbf{r}_p = \mathbf{s}_p + \mathbf{u}_p. \tag{2}$$

2.1.3 Dynamics of Multibody Systems

By calculating the kinetic energy of a flexible body with both flexible and rigid-body degrees of freedom one finds the equations of motion of a flexible body given by the matrix equation [8,9],

$$\begin{bmatrix} m_j\overline{I} & -m_j\widetilde{\mathbf{r}}_{cm,j} & \int_V \rho\overline{N}(\mathbf{s}_p)dV \\ m_j\widetilde{\mathbf{r}}_{cm,j} & \overline{J}_{t,j} & \int_V \rho\widetilde{\mathbf{r}}_p\overline{N}(\mathbf{s}_p)dV \\ (\int_V \rho\overline{N}(\mathbf{s}_p)dV)^T & (\int_V \rho\widetilde{\mathbf{r}}_p\overline{N}(\mathbf{s}_p)dV)^T & \int_V \rho\overline{N}(\mathbf{s}_p)^T\overline{N}(\mathbf{s}_p)dV \end{bmatrix} \begin{bmatrix} \dot{\mathbf{V}}_{O,j} \\ \dot{\boldsymbol{\omega}}_j \\ \ddot{\mathbf{q}}_j \end{bmatrix} = \begin{bmatrix} \mathbf{Q}_{R,j} \\ \mathbf{Q}_{\Theta,j} \\ \mathbf{Q}_{q,j} \end{bmatrix}, \tag{3}$$

or, in a simplified way,

$$\overline{M}_j\ddot{\mathbf{x}}_j = \mathbf{Q}_j, \tag{4}$$

where m_j is the mass of the flexible body j, $\mathbf{r}_{cm,j}$ the position vector of the center of mass, $\overline{J}_{t,j}$ the total inertia matrix with flexible effects, $\overline{I}$ the identity matrix, $\mathbf{V}_{O,j}$ the inertial velocity, $\boldsymbol{\omega}_j$ the angular velocity and $\mathbf{Q}_{R,j}$, $\mathbf{Q}_{\Theta,j}$ and $\mathbf{Q}_{q,j}$ the generalized force vectors for the translational, rotational and flexible degrees of freedom, respectively.

To describe the dynamics of a multibody system, the two flexible bodies j and k illustrated in Fig. 1 are considered. The body j is clamped at the $\mathbf{R}_{O,j}$ position and the body k is fixed at the end L_j of the body j. Then one can obtain the expression for the position of the body k in terms of the position vectors of the body j,

$$\mathbf{R}^i_{O,k} = \mathbf{R}^i_{O,j} + \overline{A}_{i/j}\mathbf{s}^j_{L,j} + \overline{A}_{i/j}\mathbf{u}^j_{L,j}, \tag{5}$$

where the superscript j indicates that the vector is written in the body frame j.

Performing the second derivative of Eq. 5 and describing the vectors referring to each body in its own frame of reference we find the kinematics equation for the connection between bodies according to the expression

$$\begin{aligned}\overline{A}_{i/k}\dot{\mathbf{V}}^k_{O,k} + \overline{A}_{i/k}\widetilde{\boldsymbol{\omega}}_k\mathbf{V}^k_{O,k} = \overline{A}_{i/j}\dot{\mathbf{V}}^j_{O,j} + \overline{A}_{i/j}\widetilde{\boldsymbol{\omega}}_j\mathbf{V}^j_{O,j} + \overline{A}_{i/j}\dot{\widetilde{\boldsymbol{\omega}}}_j\mathbf{s}^j_{L,j} + \\ \overline{A}_{i/j}\dot{\widetilde{\boldsymbol{\omega}}}_j\mathbf{u}^j_{L,j} + \overline{A}_{i/j}\widetilde{\boldsymbol{\omega}}_j\widetilde{\boldsymbol{\omega}}_j\mathbf{u}^j_{L,j} + 2\overline{A}_{i/j}\widetilde{\boldsymbol{\omega}}_j\dot{\mathbf{u}}^j_{L,j} + \overline{A}_{i/j}\ddot{\mathbf{u}}^j_{L,j}\end{aligned}. \tag{6}$$

Considering an array of shape functions $\overline{N}_\Theta$ that gives the flexible angular displacements $\boldsymbol{\Theta}_u$, such as $\boldsymbol{\Theta}_u = \overline{N}_\Theta\mathbf{q}$, we can describe the angular position of the body k in terms of the angular position vectors of the body j

$$\boldsymbol{\Theta}_k = \boldsymbol{\Theta}_j + \overline{N}_\Theta(L_j)\mathbf{q}_j, \tag{7}$$

which results in the kinematics equation

$$\overline{G}^{-1}_k\dot{\boldsymbol{\omega}}_k + \dot{\overline{G}}^{-1}_k\boldsymbol{\omega}_k = \overline{G}^{-1}_j\dot{\boldsymbol{\omega}}_j + \overline{N}_\Theta(L_j)\ddot{\mathbf{q}}_j + \dot{\overline{G}}^{-1}_j\boldsymbol{\omega}_j, \tag{8}$$

where $\overline{G}$ is the rotation kinematics matrix that gives the relationship between the angular velocities $\boldsymbol{\omega}_j$ and the temporal variations of the Euler angles $\dot{\boldsymbol{\Theta}}_j$ of body j, such as $\boldsymbol{\omega}_j = \overline{G}_j\dot{\boldsymbol{\Theta}}_j$.

And for the the body j that is clamped at the position $\mathbf{R}_{O,j} = \mathbf{0}$ with $\boldsymbol{\Theta}_j = \mathbf{0}$, we have the equations

$$\dot{\mathbf{V}}^j_{O,j} + \widetilde{\boldsymbol{\omega}}_j\mathbf{V}^j_{O,j} = \mathbf{0} \tag{9}$$

and

$$\overline{G}^{-1}\dot{\boldsymbol{\omega}}_j + \dot{\overline{G}}^{-1}\boldsymbol{\omega}_j = \mathbf{0}. \tag{10}$$

Grouping the Eqs. 6, 8, 9 and 10 in a system and collecting terms that depend on the accelerations $\ddot{\mathbf{x}}_j$ in a matrix $\overline{C}_q$ and the other terms in a vector $\mathbf{Q}_c$,

$$\overline{C}_q\ddot{\mathbf{x}}_j = \mathbf{Q}_c, \tag{11}$$

we obtain the definition of the kinematics of constraints in matrix form that can be inserted in the multibody dynamics.

And then, as presented in [8], the concatenation of the dynamics of the bodies is carried out and the union of the systems takes place through a system augmented by Lagrange multipliers $\boldsymbol{\lambda}$ that contains the equation of constraint kinematics described in Eq. 11, as

$$\begin{bmatrix} \overline{M}_t & \overline{C}_q^T \\ \overline{C}_q & \overline{0} \end{bmatrix} \cdot \begin{bmatrix} \ddot{\mathbf{x}}_t \\ \boldsymbol{\lambda} \end{bmatrix} = \begin{bmatrix} \mathbf{Q}_t \\ \mathbf{Q}_c \end{bmatrix}, \tag{12}$$

where $\overline{M}_t$ is the total matrix resulting from the concatenation of the body systems j and k, $\mathbf{Q}_t$ the resulting vector of forces, $\mathbf{x}_t$ the resulting vector of states and $\overline{0}$ a null matrix that completes the system.

The system described by Eq. 12 has state redundancy because the states of the rigid body of body k are fully defined by the total states of body j. Furthermore, it has extra states $\boldsymbol{\lambda}$ due to kinematic constraints. Thus, it is possible to reduce the system to only independent states $\ddot{\mathbf{x}}_i$, that is, states without dependence on other states [8]. Therefore, considering the constraints equations its possible to defined the relationship between the total states $\ddot{\mathbf{x}}_t$ and independent states $\ddot{\mathbf{x}}_i$ as:

$$\ddot{\mathbf{x}}_t = \overline{C}_{t/i}\ddot{\mathbf{x}}_i + \mathbf{Q}_{ti}. \tag{13}$$

Then, the independent multibody system can be obtained as:

$$\overline{C}_{t/i}^T\overline{M}_t\overline{C}_{t/i}\ddot{\mathbf{x}}_i = \overline{C}_{t/i}^T\mathbf{Q}_t - \overline{C}_{t/i}^T\overline{M}_t\mathbf{Q}_{ti}. \tag{14}$$

2.2 Structural Model

The flexible displacement of the structure is provided through an array of functions of the form $\overline{N}(\mathbf{s}_p)$ and depends on the approximation method adopted. There are several functions that can be used, providing different shape function matrices. Polynomials or analytically obtained modal shapes are commonly used.

2.2.1 Shape function matrix

To describe the shape function matrix, we consider the beam illustrated in Fig. 2 with its reference system with origin on the elastic axis.

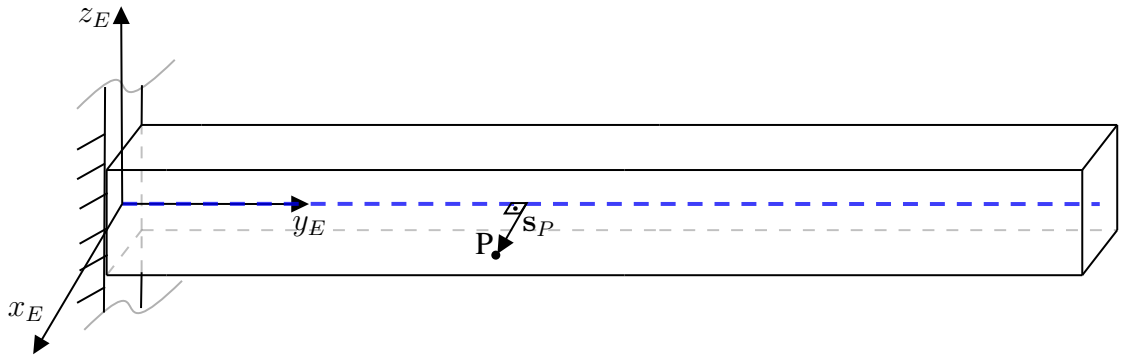

Figure 2: **Cantilever beam.** The blue dotted line describes the location of the beam's elastic axis and the vector $\mathbf{s}_P$ the position of a point P perpendicular to the elastic axis.

Considering small displacement, the flexible displacement $\mathbf{u}_E = \begin{bmatrix} u_x & u_y & u_z \end{bmatrix}^T$ of the elastic axis can be described as:

$$\mathbf{u}_E = \begin{bmatrix} N_{x,n} & 0 & 0 \\ 0 & 0 & 0 \\ 0 & N_{z,n} & 0 \end{bmatrix} \cdot \begin{bmatrix} q_{x,n} \\ q_{z,n} \\ q_{t,n} \end{bmatrix}, \tag{15}$$

or

$$\mathbf{u}_E = \overline{N}_U\mathbf{q}, \tag{16}$$

where $q_{x,n}$, $q_{z,n}$ and $q_{t,n}$ are the modal amplitudes of the nth modes of bending in x and z, and torsion about y, respectively.

In addition, the angular displacements $\mathbf{\Phi}_E = \begin{bmatrix}\phi_x & \phi_y & \phi_z\end{bmatrix}^T$ can be obtained as follows:

$$\mathbf{\Phi}_E = \begin{bmatrix} 0 & \frac{\partial N_{z,n}}{\partial y} & 0 \\ 0 & 0 & N_{t,n,i} \\ -\frac{\partial N_{x,n}}{\partial y} & 0 & 0 \end{bmatrix} \cdot \begin{bmatrix} q_{x,n} \\ q_{z,n} \\ q_{t,n} \end{bmatrix}, \tag{17}$$

or

$$\mathbf{\Phi}_E = \overline{N}_\Phi \mathbf{q}. \tag{18}$$

And then one can obtain the resulting flexible displacement at any point P described by $\mathbf{s}_P = \begin{bmatrix}x_p & 0 & z_p\end{bmatrix}^T$ as being [10],

$$\mathbf{u}_P = \left(\overline{N}_U - \widetilde{\mathbf{s}_P}\overline{N}_\Phi\right)\mathbf{q}, \tag{19}$$

then,

$$\overline{N}(\mathbf{s}_p) = \overline{N}_U - \widetilde{\mathbf{s}_P}\overline{N}_\Phi = \begin{bmatrix} N_{x,n} & 0 & z_p N_{t,n,i} \\ -x_p\frac{\partial N_{x,n}}{\partial y} & -z_p\frac{\partial N_{z,n}}{\partial y} & 0 \\ 0 & N_{z,n} & -x_p N_{t,n,i} \end{bmatrix} \tag{20}$$

2.2.2 Stiffness and damping matrices

As discussed in [8] one can describe the strain forces in terms that depend only on the flexible coordinates $\mathbf{q}$,

$$\mathbf{Q}_{d,q} = -\overline{K}\mathbf{q} - \overline{D}\dot{\mathbf{q}}, \tag{21}$$

where $\overline{K}$ is the stiffness matrix and $\overline{D}$ the damping matrix.

To obtain the stiffness matrix, the reference system coincident with the elastic axis was adopted, that is, the beam strain energy can be described as a superposition of bending and torsion strain energy without coupling terms. Therefore, the strain energy of a symmetrical beam is given by [11]:

$$U_d = \frac{1}{2}\int_0^L EI_{xx}\left(\frac{d^2u_z}{dy^2}\right)^2 dy + \frac{1}{2}\int_0^L EI_{zz}\left(\frac{d^2u_x}{dy^2}\right)^2 dy + \frac{1}{2}\int_0^L GJ\left(\frac{d\phi_y}{dy}\right)^2 dy, \tag{22}$$

where E the modulus of elasticity, I_{xx} the second moment of area of the surrounding area of the x axis, I_{zz} the second moment of area around the z axis and GJ the torsional stiffness of the beam.

Substituting the displacements for their corresponding shape functions in Eq. 22 resulting in

$$U_d = \frac{1}{2}\mathbf{q}^T\overline{K}\mathbf{q}, \tag{23}$$

where

$$\overline{K} = \begin{bmatrix} \int_0^L EI_{zz}\left(\frac{d^2N_{x,n}}{dy^2}\right)^T\frac{d^2N_{x,n}}{dy^2}dy & \overline{0} & \overline{0} \\ \overline{0} & \int_0^L EI_{xx}\left(\frac{d^2N_{z,n}}{dy^2}\right)^T\frac{d^2N_{z,n}}{dy^2}dy & \overline{0} \\ \overline{0} & \overline{0} & \int_0^L GJ\left(\frac{dN_{t,n}}{dy}\right)^2 dy \end{bmatrix}. \tag{24}$$

The damping matrix $\overline{D}$ can be obtained in several ways, such as being a proportional relationship with the mass matrix $\overline{M}_f$, with the stiffness matrix $\overline{K}$ or one between the two. In this work, the damping matrix is defined by:

$$\overline{D} = 2\xi_n \sqrt{\overline{M}_f \overline{K}}, \tag{25}$$

where ξ_n is the system damping constant.

3 NUMERICAL RESULTS

3.1 Flexible double pendulum

To verify the numerical implementation of the dynamic and structural model, a simulation of a flexible double pendulum under the effect of gravity in the initial position illustrated in Fig. 3 was performed. To perform the simulation, the software Simscape Multibody©and with the Flexible Multibody Rayleigh-Ritz model (FMBRR), developed in this work, was used. Simscape Multibody is a multibody system simulation software that uses a graphical interface of block diagrams and Euler-Bernoulli beam finite elements for flexible beam modeling.

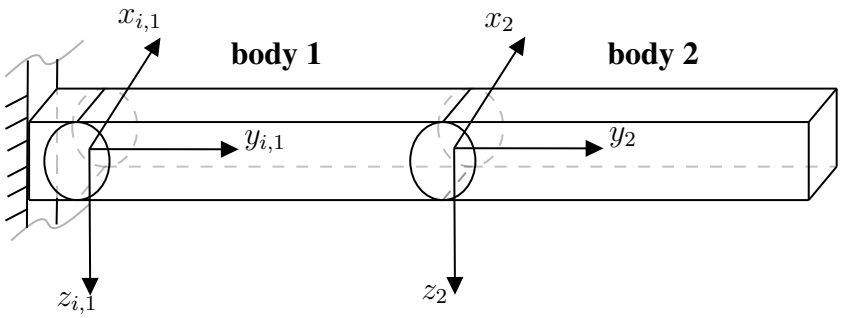

Figure 3: Illustration of the problem.

Due to the characteristics of the problem, as shown in Fig. 3, the x-axis components of the Eqs. 10 and 8 are ignored.

For the problem consider two solid beams with cross section $A_t = 0.25 \times 0.25\ m^2$, length $L = 5\ m$, density $\rho = 2700\ kg/m^3$ and simulation time of two seconds. The other properties can be found in Table 1. Both beams were discretized with 5 beam elements, in Simscape Multibody©, and 5 shape functions in ASF basis were used in the FMBRR. As an algorithm to solve the system of equations, in both simulations, **ode45** was used, an internal function of the MATLAB©, that uses the variable time step.

Table 1: Properties of each of the beams that make up the double pendulum.

Properties	Unit	Value
$\overline{J}_r$	$kg \cdot m^2$	$\begin{bmatrix} 7.0356 \cdot 10^3 & 0.0 & 0.0 \\ 0.0 & 0.0088 \cdot 10^3 & 0.0 \\ 0.0 & 0.0 & 7.0356 \cdot 10^3 \end{bmatrix}$
$\mathbf{r}_{cm}$	m	$\begin{bmatrix} 0.0 & 2.5 & 0.0 \end{bmatrix}^T$
m	kg	843.75
EI_{xx}	$Pa \cdot m^4$	$2.27865 \cdot 10^7$
EI_{zz}	$Pa \cdot m^4$	$2.27865 \cdot 10^7$
GJ	$Pa \cdot m^4$	$1.44508 \cdot 10^7$

In Fig. 4 it can be seen that the results obtained by the model of the present work are very similar to the results obtained by the software Simscape Multibody©, even with different structural methods. So, it can be said that the dynamic-structural model is coherent and properly implemented.

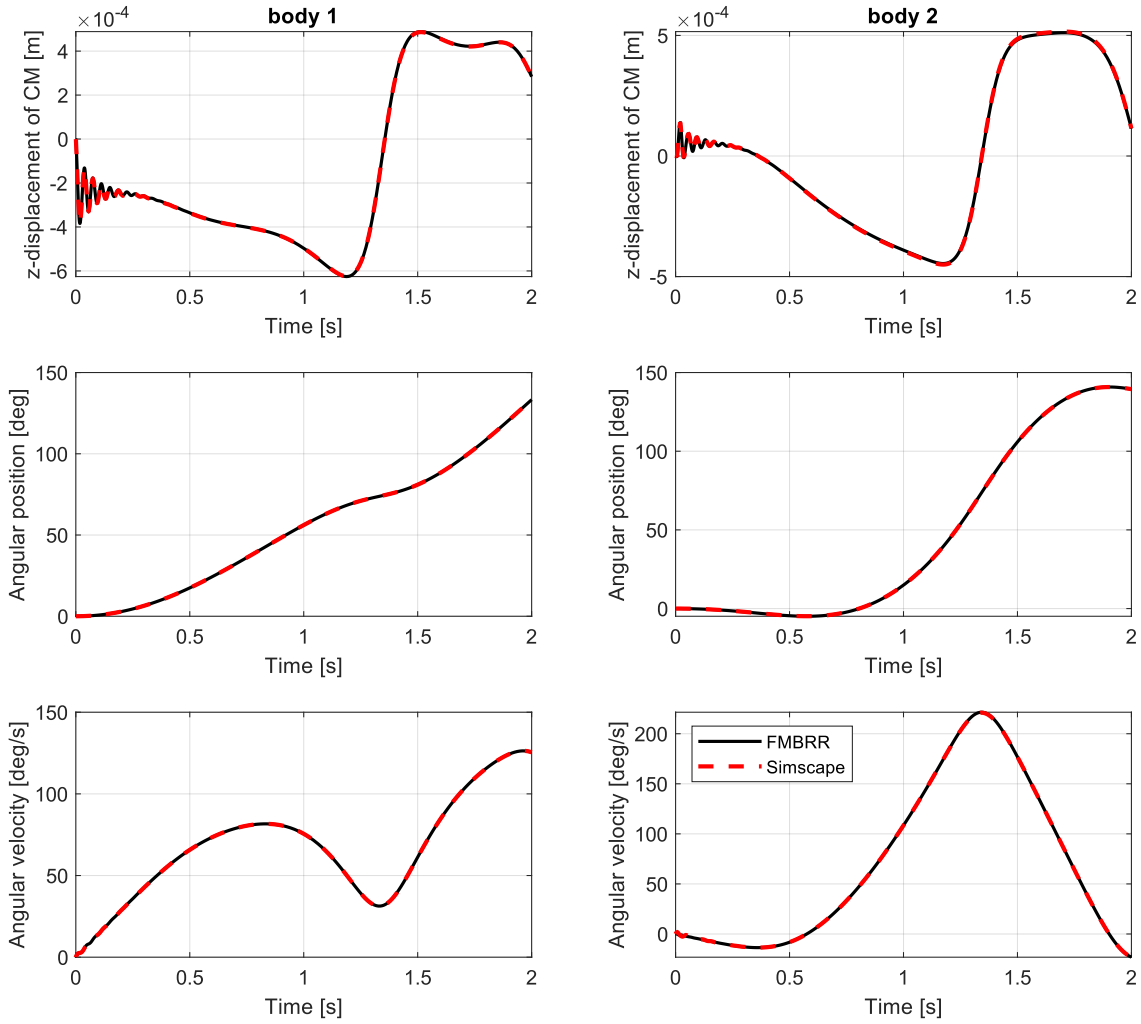

Figure 4: Comparison between the results obtained by the model and by the software Simscape Multibody©.

3.2 Very flexible beam clamped with force applied

To verify the FMBRR model for very flexible structures, the problem of a very flexible beam clamped with a vertical force F_z in a z-axis at the free end, without gravity and damping, was used. To describe the dynamics of this system, the modeling of two rigidly coupled flexible bodies presented in Subsection 2.1 was used, generalized to n bodies connected to each other. The properties of this beam are listed in Table 2, and Fig. 5 provides an illustration of the problem.

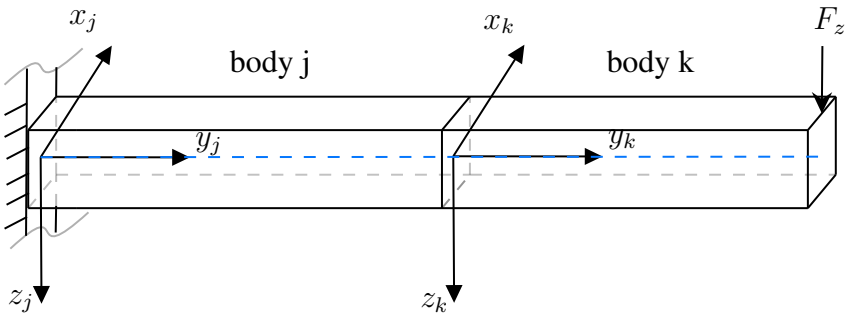

Figure 5: Clamped beam defined by 2 bodies j and k with a F_z force at the free end.

Then, as the problem has no disturbances in other axes, only the problem in the y-z plane will be analyzed, resulting in $N_{x,n} = 0$ and $N_{t,n} = 0$.

Table 2: **Beam Properties.**

Properties	Value
L	$1.0\ m$
GJ	$8.00 \cdot 10^{1}\ Nm^2$
EI_{xx}	$5.00 \cdot 10^{1}\ Nm^2$
EI_{zz}	$1.25 \cdot 10^{3}\ Nm^2$
m/L	$0.10\ kg/m$
I_{xx}	$1.30 \cdot 10^{-4}\ kgm$
I_{yy}	$5.00 \cdot 10^{-6}\ kgm$
I_{zz}	$1.25 \cdot 10^{-4}\ kgm$

To obtain an analytical modal shapes we consider an Euler–Bernoulli beam clamped, that as presented in [11], we have the modal shapes of bending in z-axis

$$N_{z,n} = \cosh\left(\frac{y}{L}\zeta_n\right) - \cos\left(\frac{y}{L}\zeta_n\right) - \frac{\sinh(\zeta_n) - \sin(\zeta_n)}{\cosh(\zeta_n) + \cos(\zeta_n)}\left(sinh\left(\frac{y}{L}\zeta_n\right) - \sin\left(\frac{y}{L}\zeta_n\right)\right), \tag{26}$$

for nth bending mode, where ζ_n is provided by the solution of the equation

$$\cosh(\zeta_n)\cos(\zeta_n) = -1. \tag{27}$$

Then, we can define the basis Analytical Shape Functions (ASF) as:

$$\mathbf{N}_{z,ASF} = \begin{bmatrix} N_{z,1} & \cdots & N_{z,n} \end{bmatrix}. \tag{28}$$

To obtain an polynomial shape functions a normalized orthogonal basis of polynomial functions that respect the boundary conditions of a clamped beam was considered, resulting in the basis Polynomial Shape Functions (PSF),

$$\mathbf{N}_{z,PSF} = \begin{bmatrix} \frac{y^2}{L^2} & -\frac{6\left(\frac{5\,L\,y^2}{6} - y^3\right)}{L^3} & \frac{28\left(\frac{15\,L^2\,y^2}{28} - \frac{3\,L\,y^3}{2} + y^4\right)}{L^4} & -\frac{120\left(\frac{7\,L^3\,y^2}{24} - \frac{7\,L^2\,y^3}{5} + \frac{21\,L\,y^4}{10} - y^5\right)}{L^5} \end{bmatrix}, \tag{29}$$

for the first four shape functions.

In Fig. 6 we can see the both $\mathbf{N}_z$ basis of shape functions. It can be said that they have a similar behavior with different magnitude and phases.

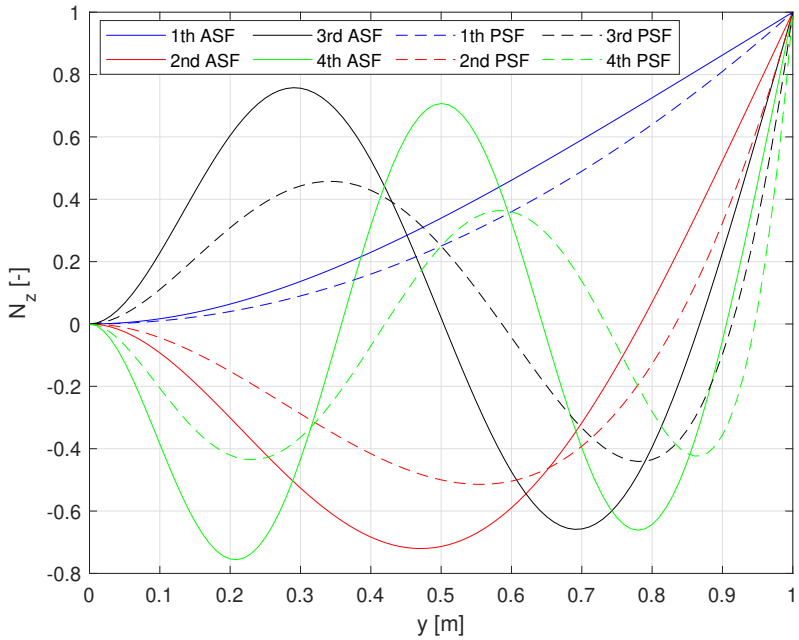

Figure 6: Comparison between analytically obtained modal shapes and polynomial shape functions, in dashed line. The 1st shape function in blue, 2nd in black, 3rd in red and 4th in green.

3.2.1 Static results

The static problem consists of finding the equilibrium condition for the beam considering different values of F_z, ranging from $5\ N$ to $145\ N$. To analyze the convergence of the results with respect to the number of shape functions in both basis, was used two cases, one with 2 bodies and other with 4 bodies. As a convergence metric the Normalized Residual Mean Square Difference (NRMSD) was used,

$$NRMSD = 100\frac{\sqrt{\frac{1}{N}\sum_{i=1}^{N}(y_i - y_{ref,i})^2}}{y_{ref,max} - y_{ref,min}}, \tag{30}$$

where y_i is the value of the vector at position i, $y_{ref,i}$ is the value of the reference vector at position i, $y_{ref,max}$ the maximum value of the reference vector and $y_{ref,min}$ the minimum value.

In Fig. 7 we can find the NRMSD value for the axial displacements, NRMSD_y, and vertical displacements, NRMSD_z for the different numbers of shape functions, n_z, for ASF and PSF. It can be analyzed that for both simulations, with 2 and 4 bodies, the PSF basis has a convergence at $n_z = 4$ with the results remaining approximately constant with the increase of n_z, a behavior not observed in the ASF basis, having a convergence at $n_z = 4$ only for the case with 4 bodies. Then, it can be concluded that the PSF basis is numerically more stable.

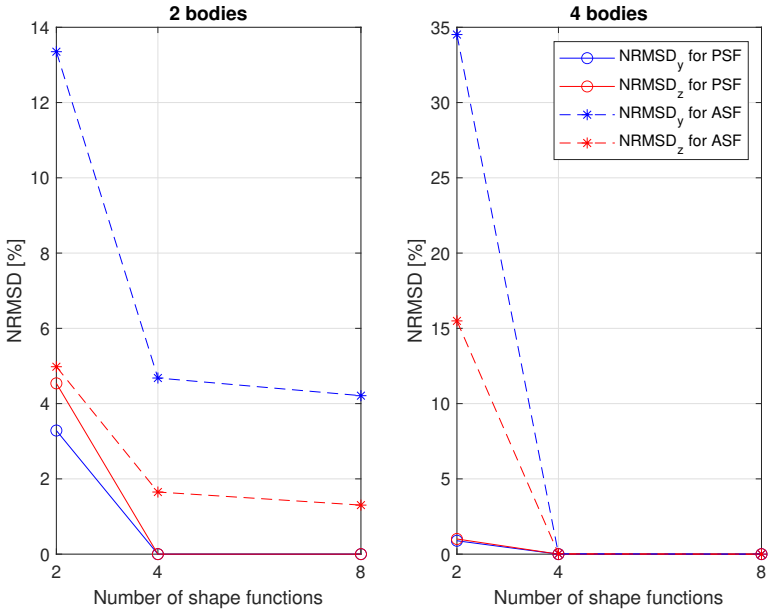

Figure 7: NRMSD for axial and vertical displacement for different number of shape functions and different number of bodies.

With the results in Fig. 7, was chosen $n_z = 4$ for basis PSF and $n_z = 8$ for basis ASF for simulation with number of bodies equal 2, 4, 6 and 8. In Fig. 8 the results for axial and vertical displacements are compared with AeroFlex model developed by [12]. It can be observed that only the PSF converges to the results of AeroFlex, while the ASF gives the same results for 2 and 4 bodies but when the number of bodies increase the result diverges. This behavior can be more easily observed in Fig. 9 which has the NRMSD values based on AeroFlex.

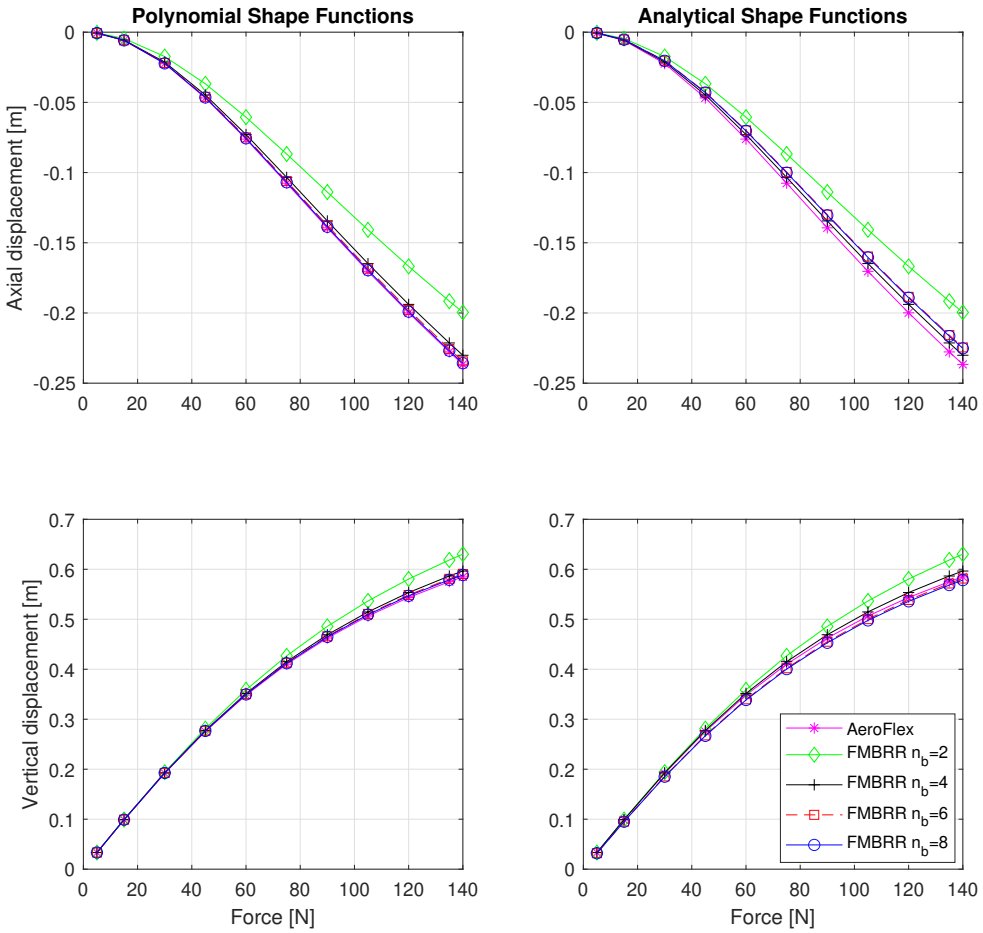

Figure 8: Axial and vertical displacement at the free end of the beam as a function of the force applied F_z.

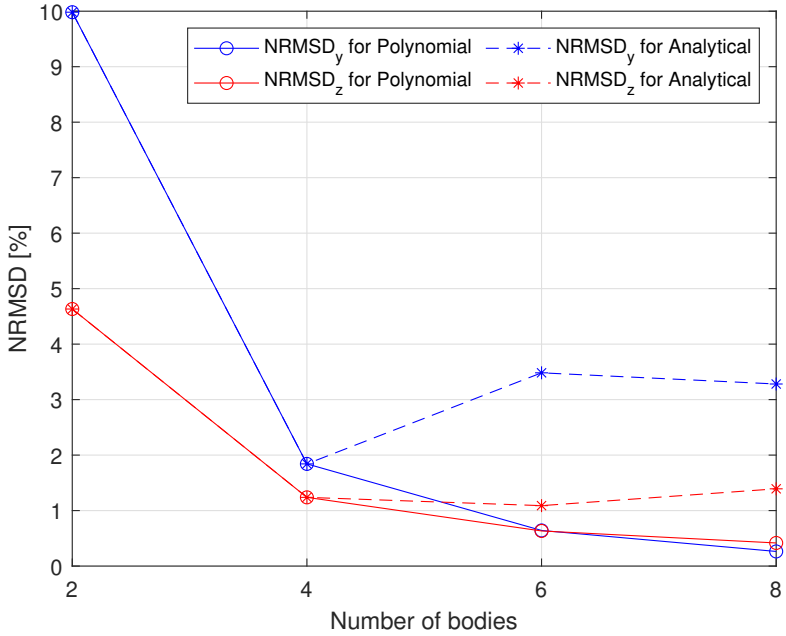

Figure 9: NRMSD for axial and vertical displacement for different number of bodies.

With the static results obtained, it can be concluded that the PSF basis is more numerically stable, providing faster convergence based on the number of functions and also converging to the reference result with a smaller number of functions in comparison to ASF. Furthermore, it was noted that the ASF function base has a numerically unstable behavior, changing its convergence behavior with the change in the number of bodies.

3.2.2 Dynamic results

The dynamic problem consists of $1\ s$ simulation with $F_z = 10\sin(20t)$, without gravity and damping. Similar to static problem, was chosen $n_z = 4$ for basis PSF and $n_z = 8$ for basis ASF for simulation with number of bodies equal 2, 4, 6 and 8. As an algorithm to solve the system of equations the **ode45** was used, an internal function of the MATLAB©, that uses the variable time step.

To compare the Augmented Multibody System (AMS), defined in Eq. 12, and Independent Multibody System (IMS), defined in Eq. 14, a simulation was performed with 4 bodies and PSF basis. The result is found in Fig. 10 and it can be conclude that the both approach give approximately the same results, but the IMS has error in position of the constraints more stable numerically.

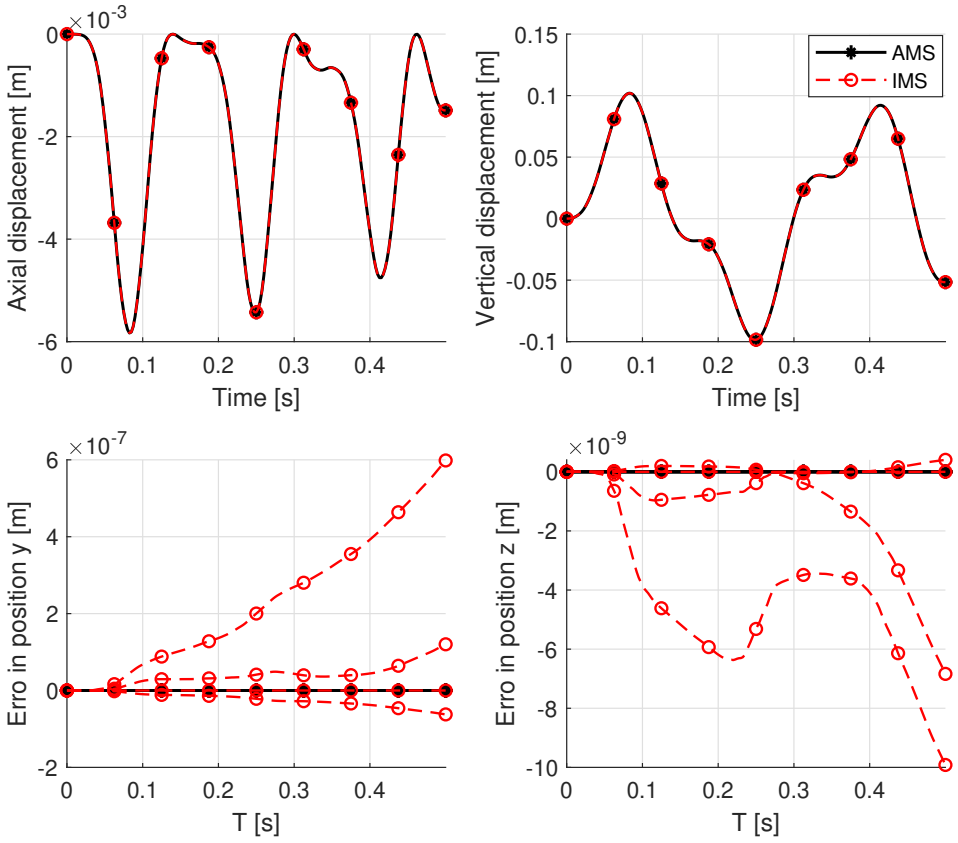

Figure 10: Axial and vertical displacement at the free end and error in position in y and z for 4 bodies simulation. Comparison with AMS and IMS.

In Fig. 11 the results for axial and vertical displacements are compared with AeroFlex. Analyzing the results, it is observed that the applied force was not enough to generate large geometric

nonlinearities, that is, the magnitude of the vertical displacement is much greater than the magnitude of the axial displacement. Then, it is observed that the result for the vertical displacement does not change with the increase in the number of bodies, while for the axial displacement a convergence is observed with the increase in the number of bodies using the PSF basis. Furthermore, there is once again a difficulty in convergence using the ASF basis.

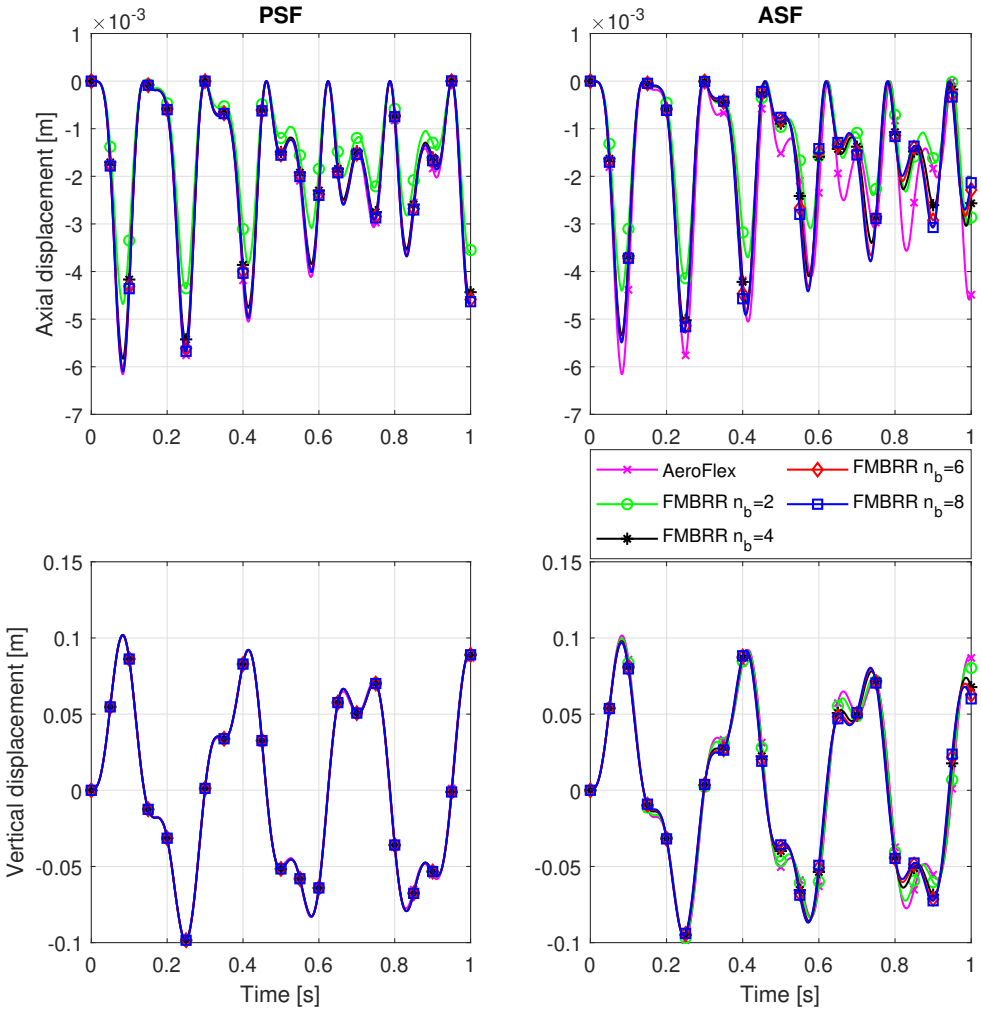

Figure 11: Axial and vertical displacement at the free end of the beam as a function of time.

4 CONCLUSION

In this work, a framework was developed using flexible multibody modeling coupled with structural modeling using the Rayleigh-Ritz method capable of describing geometric nonlinearities in very flexible structures, despite using a linear structural model. Furthermore, it presents versatility to describe different structures with different types of connection, requiring only the modification of the constraint matrix.

Furthermore, comparisons were made between two different function basis, where it was noted that there was a difficulty in using a base of trigonometric functions derived from the analytical result of the problem of a free unforced fixed beam, called as ASF, to solve the problem with large displacements. However, when using the base of polynomial functions proposed by this

work, called PSF, this difficulty was not observed, providing numerically stable results. Also, two different modeling of the multibody system were compared, where it was observed that the IMS modeling provided greater numerical stability of the constraints, however, the result obtained by both is very similar, since the instability presented in the AMS modeling does not was relevant to the proposed problem.

Ongoing and future work focuses on integrating the framework with vortex lattice method and unsteady strip theory. In particular, the multibody approach appears to be a promising method for modeling and simulating highly flexible wings with folding wingtips. Further analysis will investigate the effects of geometrically nonlinear flexible dynamics and folding wingtip dynamics on aircraft stability. Additionally, the design of active and passive control laws to reduce aircraft loads using folding wingtips is under development, aiming to enhance aircraft performance and safety.

ACKNOWLEDGMENTS

This study was financed in part by Finep and Embraer S.A. under the research project "Advanced Studies in Flight Physics and Control" - contract number 01.22.0552.00, and in part by the *Coordenação de Aperfeiçoamento de Pessoal de Nível Superior - Brasil* (CAPES) - Finance Code 001.

5 REFERENCES

[1] Guimarães Neto, A. B., Silvestre, F. J., Cardoso-Ribeiro, F. L., et al. (2017). Validity of the assumption of small deformations in aircraft with different levels of structural flexibility. In *The International Forum on Aeroelasticity and Structural Dynamics*. Como, Italy: The International Forum on Aeroelasticity and Structural Dynamics, p. 80.

[2] Cesnik, C. E. S., Senatore, P. J., Su, W., et al. (2012). X-hale: A very flexible unmanned aerial vehicle for nonlinear aeroelastic tests. *AIAA Journal*, 50(12), 2820–2833.

[3] Su, W. (2008). *Coupled Nonlinear Flight Aeroelasticity and Flight Dynamics of Fully Flexible Aircraft*. Dissertation for a doctoral degree, The University of Michigan, Ann Arbor, Michigan.

[4] Brown, E. L. (2003). *Integrated Strain Actuation In Aircraft With Highly Flexible Composite Wings.* Dissertation for a doctoral degree, Massachusetts Institute of Technology, Cambridge, Massachusetts.

[5] Shearer, C. M. (2006). *Coupled Nonlinear Flight Dynamics, Aeroelasticity and Control of Very Flexible Aircraft.* Dissertation for a doctoral degree, The University of Michigan, Ann Arbor, Michigan.

[6] Zhao, Z. and Ren, G. (2011). Multibody dynamic approach of flight dynamics and nonlinear aeroelasticity of flexible aircraft. *AIAA Journal*, 49(1), 41–54.

[7] Kruger, W. R. (2007). Multibody dynamics for the coupling of aeroelasticity and flight mechanics of highly flexible structures. In *Stockholm: International Forum on Aeroelasticity and Structural Dynamics.* Stockholm: International Forum on Aeroelasticity and Structural Dynamics.

[8] Shabana, A. A. (2005). *Dynamics of multibody systems*. Cambridge University Press, 3rd ed ed. ISBN 978-0-521-85011-7.

[9] Orzechowski, G., Matikainen, M. K., and Mikkola, A. M. (2017). Inertia forces and shape integrals in the floating frame of reference formulation. *Nonlinear Dynamics*, 88, 1953–1968.

[10] Branlard, E. S. P. (2019). Flexible multibody dynamics using joint coordinates and the rayleigh-ritz approximation: The general framework behind and beyond flex. *Wind Energy*, 22, 877–893.

[11] Bisplinghoff, R. L. and Ashley, H. (2002). *Principles of Aeroelasticity*. Dover Phoenix Editions. Dover Publications. ISBN 9780486495002.

[12] Ribeiro, F. L. C., Paglione, P., da Silva, R. G. A., et al. (2012). Aeroflex: a toolbox for studying the flight dynamics of highly flexible airplanes. In *VII Congresso Nacional de Engenharia Mecânica*. VII Congresso Nacional de Engenharia Mecânica.

COPYRIGHT STATEMENT